Ultramicroscopy 159 (2015) 81–94

Contents lists available at ScienceDirect

Ultramicroscopy

journal homepage: www.elsevier.com/locate/ultramic

Introduction and comparison of new EBSD post-processing methodologies

Stuart I. Wright [a,*], Matthew M. Nowell [a], Scott P. Lindeman [a], Patrick P. Camus [b], Marc De Graef [c], Michael A. Jackson [d]

[a] EDAX, 392 East 12300 South, Suite H, Draper, UT 84020, USA
[b] EDAX, 91 McKee Drive, Mahwah, NJ 07430, USA
[c] Carnegie Mellon University, Department of Material Science and Engineering, 5000 Forbes Avenue, Pittsburgh, PA 15213, USA
[d] BlueQuartz Software, 400 S. Pioneer Blvd, Springboro, OH 45066, USA

ARTICLE INFO

Article history:
Received 18 May 2015
Received in revised form
7 July 2015
Accepted 16 August 2015
Available online 17 August 2015

Keywords:
Electron Backscatter Diffraction
EBSD

ABSTRACT

Electron Backscatter Diffraction (EBSD) provides a useful means for characterizing microstructure. However, it can be difficult to obtain index-able diffraction patterns from some samples. This can lead to noisy maps reconstructed from the scan data. Various post-processing methodologies have been developed to improve the scan data generally based on correlating non-indexed or mis-indexed points with the orientations obtained at neighboring points in the scan grid. Two new approaches are introduced (1) a re-scanning approach using local pattern averaging and (2) using the multiple solutions obtained by the triplet indexing method. These methodologies are applied to samples with noise introduced into the patterns artificially and by the operational settings of the EBSD camera. They are also applied to a heavily deformed and a fine-grained sample. In all cases, both techniques provide an improvement in the resulting scan data, the local pattern averaging providing the most improvement of the two. However, the local pattern averaging is most helpful when the noise in the patterns is due to the camera operating conditions as opposed to inherent challenges in the sample itself. A byproduct of this study was insight into the validity of various indexing success rate metrics. A metric based given by the fraction of points with CI values greater than some tolerance value (0.1 in this case) was confirmed to provide an accurate assessment of the indexing success rate.

1. Introduction

In general, images or maps reconstructed from automated Electron Backscatter Diffraction (EBSD) data provide an excellent way to characterize the orientation aspects of polycrystalline microstructures [1]. This technique is also referred to as Orientation Imaging Microscopy or OIM [2]. However, some EBSD maps can be noisy, with a large fraction of non-indexed or mis-indexed points in the scan grid. Noisy maps generally arise when patterns are too noisy for the automated band detection and indexing algorithms to work reliably. Noisy patterns can arise for various reasons, for example highly deformed materials and fine-grained materials tend to produce patterns of lower quality due to resolution limitations related to the size of the interaction volume and the fine scale of the structure in such materials. Another source of noise is the EBSD camera itself. While higher speed data collection is desirable, the camera settings often required to achieve higher speeds – higher gain and shorter exposure times – can lead to degraded pattern quality. While the band detection (i.e. the Hough Transform) and indexing routines can overcome quite a lot of noise in the patterns, the reliability of these algorithms begins to diminish as was recognized early in the development of the automated technique [3,4].

Various post-processing approaches have been developed to try and cleanup the orientation data in an attempt to improve the fidelity of the EBSD maps relative to the underlying microstructure [5,6]. These techniques tend to lead to high levels of artifacts as the fraction of non-indexed or incorrectly indexed points becomes large. Often, scan fidelity can be improved by adjusting various parameters during offline re-scanning of the the data using EBSD

Abbreviations: CI, Confidence Index; EBSD, Electron Backscatter Diffraction; ES, Extra Solutions; IPF, Inverse Pole Figure; ISR, Indexing Success Rate; ISR^{CI}, Fraction of points in a scan with CI values greater than 0.1 after CI Standardization; ISR^{R}, Fraction of points in a scan within 5° of a reference scan; ISR^{RK}, Fraction of points in a scan within 5° of a reference scan with kernel searching; KAM, Kernel Average Misorientation; NPAR, Neighbor Pattern Averaging and Re-indexing; PPS, Points Per Second referring to the a scan rate

* Corresponding author.

http://dx.doi.org/10.1016/j.ultramic.2015.08.001

patterns recorded during the original online scan. For example, image processing can be applied to the saved patterns in order to improve the indexing, mistakes made in defining the crystallographic structure parameters used in indexing can be corrected, the pattern center calibration improved and Hough Transform parameters better optimized for the patterns collected. Such adjustments allow the patterns to be re-indexed to improve on the original results.

In this work, we introduce two new post-processing approaches to improve scan fidelity when the incoming patterns are of poor quality. As with most cleanup approaches, these new approaches use data from neighboring points in an attempt to improve the scan results. The first is a re-indexing approach which averages the patterns of neighboring points in the scan grid prior to indexing. The second uses the results from the voting step in the triplet indexing scheme. These results are compared both to conventional scanning (and re-scanning) results, to a novel pattern matching approach [7], and to the established grain dilation cleanup routine [6].

2. Materials

The post-processing methodologies are compared for four different materials. It should be noted that no frame averaging was used during collection of the patterns. In all four cases, the patterns were collected and recorded after background correction. All data was collected using an EDAX Hikari Super camera on an FEI XL-30 field emission gun SEM.

2.1. Duplex steel with artificial noise

The first sample is a 2205 duplex steel sample with a recrystallized microstructure. Nearly 130,000 points were scanned on a hexagonal grid with a 200 nm step size. The EBSD pattern at each point was saved. The dimensions of the patterns were 96×96 pixels. The Hough was performed on the original 96×96 pixel patterns with a 9×9 convolution mask, 1° theta step size and searching for a maximum of 10 peaks. Varying levels of Gaussian noise were added to the patterns. This was done by calculating an intensity ranging from -255 to $+255$ for each pixel in the pattern, such that the distribution of these intensities over all pixels in the pattern formed a Gaussian distribution centered at 0. This intensity was multiplied by a factor ranging from 0 to 1 and then added to the original intensity of the pixel.

2.2. NI with varied camera conditions

The second sample was an Inconel 600 nickel alloy sample with a recrystallized microstructure. Ten scans were run repeatedly over the same area in the sample. With each scan, the pattern quality was degraded by operating the camera with increasing electronic gain ranging from the minimum on the camera to the maximum (0, 9.0, 18.0, 22.5, 27.0, 28.2, 29.3, 30.4 31.5 and 36.0 dB) and decreasing exposure times (8.03, 2.78, 0.94, 0.55, 0.32, 0.27, 0.23, 0.20 and 0.17 ms). The patterns were collected at 60×60 pixels. The Hough was actually performed on the 60×60 pixel patterns stretched to 80×80 pixels with a 9×9 convolution mask, a 2° theta step size and searching for a maximum of 9 peaks. The data was collected on a square scan grid.

2.3. Deformed Mg

The third sample was a heavily deformed magnesium sample. This sample was scanned with a gain at approximately 25% of the maximum for the camera and at a rate of 233 points per second on hexagonal grid. Patterns with pixel dimensions of 114×114 were collected and recorded. The Hough was run on the patterns after compression to 96×96 pixels with a 9×9 convolution mask, 1° theta step size, and searching for a maximum of 10 peaks.

2.4. Piano wire

The fourth sample was low-carbon steel piano wire sample with a fine grain size – approximately 250 nm [8]. This sample was scanned twice over two different areas with two different gains settings on the camera. The first scan was collected at 54 points per second with a gain of 0 and the second at 154 points per second at a gain of 25% of the maximum. 96×96 pixel patterns were collected and recorded. The Hough was run at the same 96×96 pixel resolution with a 9×9 convolution mask, 1° theta step size, and searching for a maximum of 10 peaks. The data was collected on a hexagonal scan grid.

3. Methods

3.1. Conventional re-scans

Each of the datasets were re-scanned using the recorded patterns using the Hough Transform [4] and triplet indexing [3] routines as implemented in version 7.2.1 of the EDAX OIM DC software.

3.2. Extra solutions (ES) cleanup

The triplet indexing technique uses a voting scheme to determine the most probable indexing solution to a pattern [3]. For each triplet of bands that can be formed from the detected bands (120 for 10 bands), all possible indexing solutions satisfying the angles between each of the pairs of the bands in the triplet are determined. This is done by comparing the angles against a set of pre-calculated look-up-table of interplanar angles generated from the strongest diffracting planes in the crystal lattice. In addition to matching the angles within a given tolerance (3° was used in all cases) the indices of the planes must also pass a logic test. The possible solutions for all of the triplets are gathered together and the most frequently appearing solution is assumed to be the correct indexing solution to the pattern. The key feature of this approach, in terms of the extra solutions cleanup method, is that multiple solutions are found for each pattern. The indexing software has been modified to record the top three solutions (in terms of number of votes) at each point in the scan. During post processing, points with low confidence indexes (CI) [9] are examined. If a point is found to have a low CI (we have used 0.1 as the cutoff value in the cases shown here) then the other two “extra” solutions are examined to see if they match the orientations of any of the neighboring points in the scan grid. The orientation of the current point is then assigned the orientation of the “extra” two solutions that appears most often among the neighboring scan points. If neither of the two “extra” solutions is found then the current point retains its original orientation.

3.3. Neighbor pattern averaging with re-indexing (NPAR)

For each point in a scan, the corresponding pattern is averaged with the patterns of the four neighboring scan points as shown schematically in Fig. 1.

$$\overline{I_{ij}^{x,y}} = \frac{1}{5}\left(I_{ij}^{x,y} + I_{ij}^{x-\Delta x,y} + I_{ij}^{x+\Delta x,y} + I_{ij}^{x,y-\Delta y} + I_{ij}^{x,y+\Delta y}\right) \quad (1)$$

$I_{ij}^{x,y}$ is the intensity in the pattern at pixel coordinate i, j for the

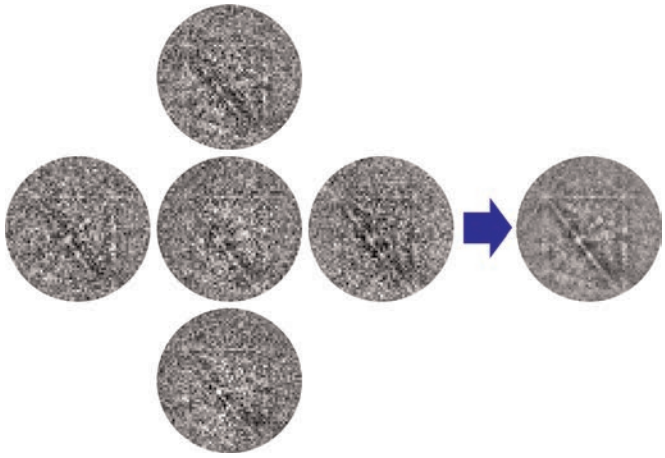

Fig. 1. Schematic of the averaging of the pattern at a given point with the patterns of the neighboring points.

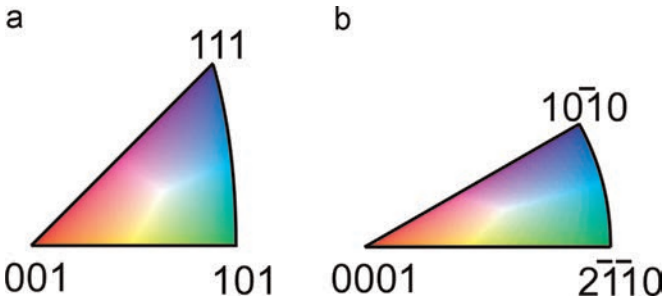

Fig. 2. Orientation map color keys for the (a) duplex steel, nickel alloy and piano wire samples and (b) the deformed magnesium sample.

point in the scan with coordinates x, y. Δx and Δy denote the step sizes between neighboring points in the grid in the horizontal and vertical directions (they are equal in all the cases shown here).

If the data is collected on a hexagonal grid then the averaging kernel contains the pattern of the point of interest and the patterns of the six nearest neighbors.

One concern of the NPAR methodology is that it leads to a potential loss in spatial resolution. This concern will be discussed as the different results are presented.

3.4. Dictionary method

Another approach to indexing is to compare an experimental pattern against a dictionary of simulated patterns and find the best match. We have used this approach simply as an independent method of indexing for comparison purposes for the nickel sample.

This approach has been realized [7] using dynamical simulations of EBSD patterns. 333,227 patterns were simulated over a set of orientations encompassing the full asymmetric domain of orientation space for cubic symmetry. Comparing each pattern in the scan grid against all of the patterns in the dictionary is computationally intensive. In addition, the forward modeling of the dynamical EBSD scattering process is computationally intensive as well, in particular for lower symmetry materials, due to the very large number of scattered beams that need to be taken into account For the simulations performed in this study a 20 keV incident energy was used to match that used on the SEM. 31 Monte Carlo energy bins from 5 keV to 20 keV were used and the simulated patterns are weighted averages over the 31 individual patterns. The simulations are done over the full surface of the detector (480×480 pixels) and then binned down to match that recorded experimentally. Random Poisson noise was added prior to binning. A more detailed description of the method is given in the cited paper.

3.5. Indexing success rate (ISR)

The indexing success rate is a helpful way of comparing results from the different post-processing methodologies presented. One can imagine several ways of measuring the fraction of correctly indexed points during an automated EBSD scan. However, two methods are generally most common depending on the type of EBSD system used to collect the data. For Oxford and Bruker systems the indexing success rate is often given in terms of the fraction of zero solutions. Zero solutions are points in the scan for which no indexing solution could be found for the corresponding pattern. With EDAX (or formerly TSL) systems, the triplet indexing approach tends to find a solution for nearly every point in the scan, thus a zero solution approach would be unsound. However, the confidence index (CI) provides a measure of indexing reliability [9]. Thus, an indexing success rate can be defined as the fraction of points with a CI greater than a specified tolerance value (0.1 or 0.2 are typical). Points at grain boundaries tend to have very low CI values even though they may be correctly indexed with orientations matching either of the orientations of the grains separated by the boundary. A CI upgrade technique has been devised termed CI standardization [10] which resolves the improper exclusion of points with low CI values but with orientations similar to their neighbors. It should be noted that this technique only modifies the CI values, the crystallographic orientations remain unchanged. Calculating the fraction of points with CIs greater than a specified tolerance value (we have used 0.1 exclusively in this work) after CI standardization provides a metric for the indexing success rate. We will designate this metric ISR^{CI}.

Another approach used in this work is to compare a given scan against a reference scan on a point-by-point basis. If an angular tolerance (we have used 5°) is set then the indexing success rate can be given as the fraction of points in the test scan having orientations within this tolerance value of the orientations of the corresponding points in the reference scan. We will term this approach ISR^{R}. One failing of this approach is that for a point at a grain boundary the orientation obtained can easily be associated with the grain on either side of the boundary. The choice of which grain orientation to select is somewhat arbitrary when the amount of each grain within the interaction volume is nearly the same. A boundary point may be correct in the sense that it matches the orientation of one of the neighboring grains but does not match the orientation for the same boundary point in the reference scan where an alternate, yet equally correct, solution was selected. To overcome this, a point in a scan will not only be compared to the identical point in the reference scan but also compared against any of the orientations in the kernel of neighboring points in the reference scan. If a match is found within the kernel then the point is considered correct. It should be noted that we only perform the kernel search in the results from the reference scan and not conversely in the comparison scan. We designate this kernel search modification as ISR^{RK}. It should be noted that if this kernel searching approach were used in the test scan as opposed to the reference scan it would lead to significant inflation of the ISR. However, as shown in Section 4.1.2, the use of the kernel searching solely in the reference scan leads to valid ISR measurements.

Other metrics for the ISR include the fraction of points with pattern quality, mean angular deviation, fit or other parameters less or greater than some tolerance as appropriate for the discriminating parameter. However, in this work we limit the indexing success rate metrics to the four previously described.

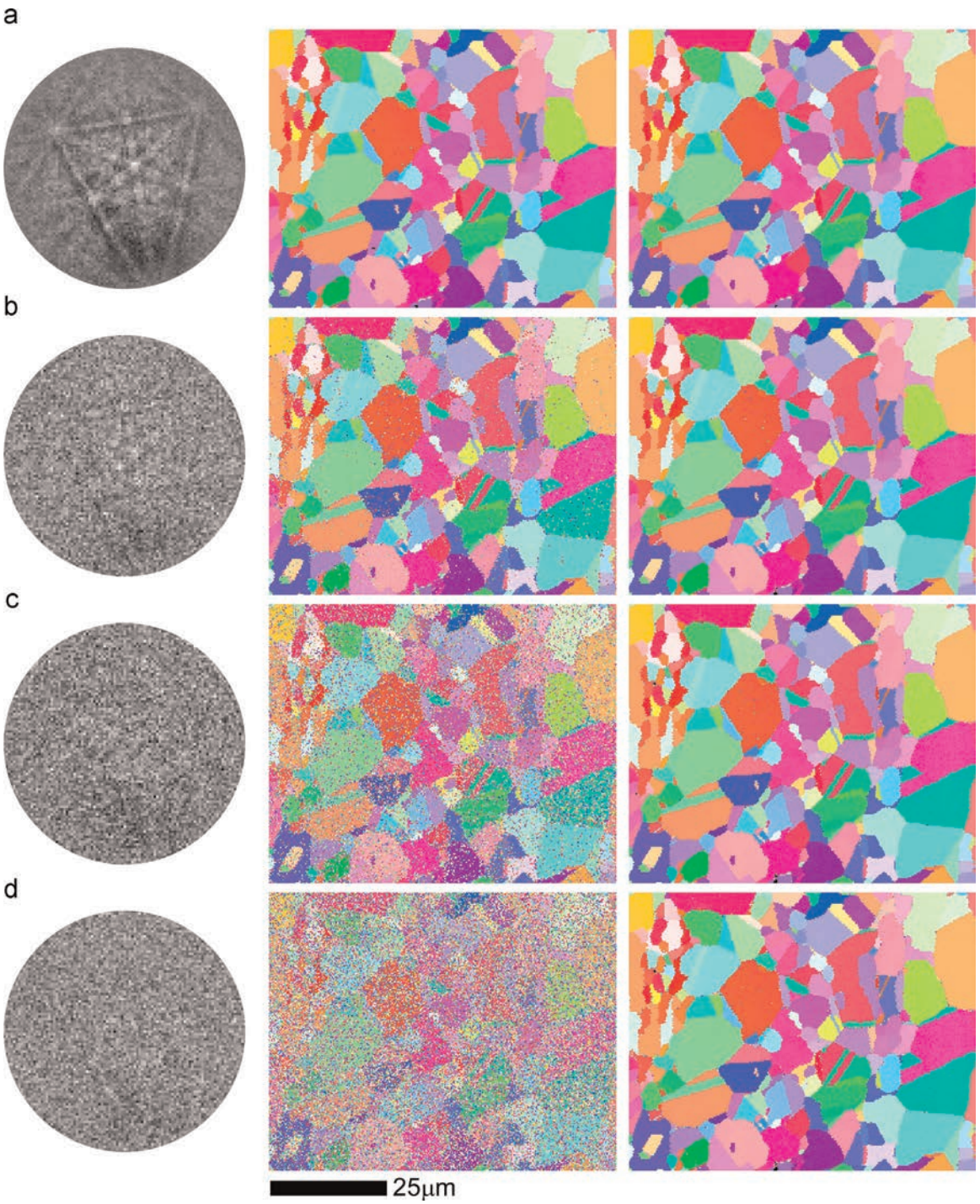

Fig. 3. Example pattern with noise added and orientation maps obtained after conventional and NPAR re-scanning for patterns with noise levels of (a) 0, (b) 0.5, (c) 0.8, (d) and 1.0.

4. Results and discussion

The orientation maps shown in subsequent sections are sometimes referred to as Inverse Pole Figure or IPF maps. In these maps, the color designates the crystal direction parallel to the sample normal according to the color keys shown in Fig. 2.

4.1. Duplex steel with artificial noise

4.1.1. Mapping results

Fig. 3 shows results for the duplex steel sample with artificial noise applied to the patterns after which the noisy patterns are re-scanned using both the conventional and NPAR approaches. The NPAR approach clearly provides a significant improvement to the fidelity of the resultant maps.

ES cleanup was also applied to the noisy pattern results and provided some improvement but not nearly as dramatic as that achieved with the NPAR method. The maps after ES cleanup were not included in Fig. 3 as the improvements were too subtle to be clearly observable.

4.1.2. Indexing success rates

For the sake of comparison, we use the as-scanned dataset as the reference scan for the indexing success rate calculations on

Table 1
Indexing success rates for the post-processing of nickel data with artificial noise added.

Noise level	Conventional re-scan			ES cleanup			NPAR		
	ISR^{CI} (%)	ISR^{R} (%)	ISR^{RK} (%)	ISR^{CI} (%)	ISR^{R} (%)	ISR^{CI} (%)	ISR^{CI} (%)	ISR^{R} (%)	ISR^{RK} (%)
0.0	99.8	100	100	99.8	100	100	99.8	97.0	99.8
0.5	96.7	96.2	96.8	97.4	96.6	97.4	99.7	96.8	99.7
0.6	92.0	91.7	92.2	93.7	83.1	93.7	99.6	96.7	99.6
0.7	81.6	81.9	82.2	86.0	85.7	86.3	99.5	96.6	99.4
0.8	65.2	66.7	66.9	73.2	73.7	74.1	99.2	96.5	99.2
0.9	45.4	50.0	50.1	56.6	59.1	59.4	98.9	96.2	98.9
1.0	24.0	23.8	23.8	35.9	43.9	44.1	98.5	95.9	98.5

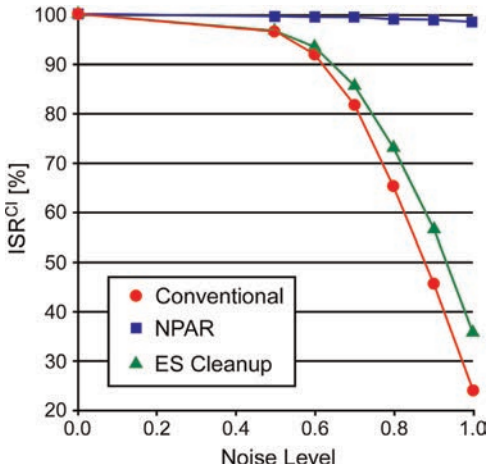

Fig. 4. Plot of the indexing success rates as a function of the noise level.

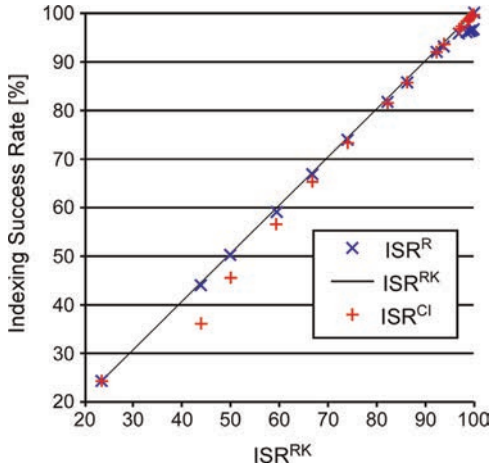

Fig. 6. Plot of the various ISR metrics as a function of ISR^{RK} for the data in Table 1.

this sample. Table 1 shows a summary of the ISRs obtained for the maps shown in Fig. 3.

If we plot the ISR^{CI} data for the conventional re-scan, ES cleanup and NPAR results as shown in Fig. 4, we see that the ES cleanup does provide a moderate improvement on the indexing success rate particularly at the higher noise levels. However, as the maps show as well the NPAR method provides much more significant improvement in the indexing success rate.

As noted in Section 3, the indexing success rate metric ISR^{R} based on a point-to-point comparison of orientations between the comparison results and the reference scan results has the potential to underestimate the indexing success rate because of the inherent

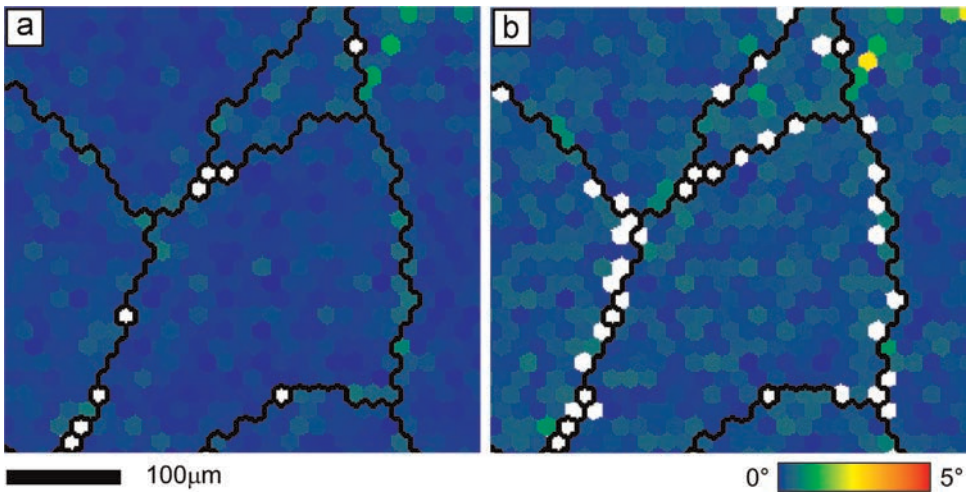

Fig. 5. Point-by-point comparison maps for the NPAR results on 0.5 noise level scan and the reference scan, i.e. the conventional scan on the as-collected patterns. (a) With kernel searching and (b) without kernel searching. Boundaries greater than 5° are overlaid in black and points in white are unmatched.

Table 2
Average KAM values for the different post-processing methodologies and noise levels.

Noise	Conventional re-scan (°)	ES cleanup (°)	NPAR (°)
0	0.32	0.33	0.19
0.5	0.72	0.73	0.37
0.6	0.86	0.88	0.42
0.7	1.00	1.06	0.45
0.8	1.16	1.26	0.49
0.9	1.33	1.48	0.53
1.0	1.48	1.67	0.57

ambiguity in the indexing deconvolution at grain boundaries. Fig. 5 shows this effect clearly. In this map the angular deviation between the 0.5 noise level NPAR scan is compared against the reference scan pixel by pixel. Deviations near 0° are colored blue and range through yellow to red at a maximum of 5°. Points with deviations greater than 5° are shaded white. In Fig. 5a the white points are concentrated at the boundaries where the indexing selection ambiguity is most prevalent. Fig. 5b shows the comparison results with kernel searching; there are still a few white points at the boundaries but considerably less. However, it is also clear from comparing the two maps that deviations in the grain interiors decrease with kernel searching as well as would be expected.

Fig. 6 compares the different metrics for quantifying the indexing success rate. In general, the CI based approach to measuring the index success rate (ISR^{CI}) becomes increasingly conservative with decreasing scan quality. When the indexing rate is high ($>90\%$) ISR^{CI} is nearly the same as ISR^{RK}. ISR^{R} and ISR^{RK} are nearly identical until the indexing rate is high, where the ISR^{R} drops below ISR^{RK} as expected. The plot in Fig. 6 and the fact that all missed points in Fig. 5 are at the grain boundaries suggests that not including the kernel search leads to a slight deflation in the true ISR as opposed to an artificial inflation when using the kernel search.

4.1.3. Grain boundaries

Indexing problems tend to concentrate around grain boundaries. This is due to the volume of interaction of the electron beam with the sample. In the immediate vicinity of a grain boundary, the interaction volume will contain atoms from the crystal lattices of the two grains on either side of the grain boundary. This leads to a diffraction pattern which is essentially a mix of the two diffraction patterns from the two crystal lattices. The mixed pattern can lead to challenges for the indexing algorithm as discussed in detail by Wright et al. [11]. As NPAR increases the virtual interaction volume, this could actually lead to a greater fraction of mixed boundaries leading to a lower overall ISR. However, this was not observed in these results. It is assumed that the beneficial contribution of neighboring points from the same crystal lattice overwhelms the negative aspects of mixing in patterns from the other crystal lattice at the grain boundaries. It should be noted, however, that as the step size is increased relative to the underlying grain size the fraction of points at the grain boundaries (and triple junctions) increases as well. For example, for a scan performed on a square or hexagonal grid a circular grain with a diameter equal to 10 grid points, the fraction of grid points at the boundary of the circle relative to the number of total points in the circle is 0.35. For a circle with a diameter equal to 5 grid points, the boundary fraction is 0.57 for a square grid and 0.63 for a hexagonal grid. Thus, as the step size increases, there will be more mixing of patterns leading to a reduction in the benefits of neighbor pattern averaging and for very coarse grids where there is perhaps only a single point per grain on average (as may be the case in nanostructured materials or in scans done solely for texture evaluation) NPAR would degrade the results and would be inappropriate.

It should also be noted that the noise added to the patterns is applied equally to patterns from points in the grain interiors and to patterns from points adjacent to grain boundaries. While this likely does not reflect true pattern noise, the pattern mixing effect at grain boundaries was already present in the original patterns and, thus, it is assumed that any effects from the equal application of noise to the patterns would be negligible.

4.1.4. KAM results

One measure of orientation precision is the degree of local misorientation within the scan results [11]. This can be characterized using the kernel average misorientation (KAM) [12,13]. In a recrystallized material such as the nickel sample investigated, we expect the KAM values to approach zero. Average KAM values for the different scans are summarized in Table 2. The KAM values listed in the table were calculated for first nearest neighbor kernels with a 5° maximum misorientation. The table shows that the NPAR method decreases the KAM values. In general, the improved KAM values could be due to improved precision arising from higher quality patterns or alternatively it could be due to a smearing effect where slightly different patterns are smeared together leading to a smoothing of the resultant orientation data. However, the latter case would only be applicable for a deformed material. It is interesting to note that ES cleanup tends to increase the KAM values. However, this is expected. When the initial orientation solution is angularly distant from the orientations of the neighboring points it is excluded from the KAM calculation

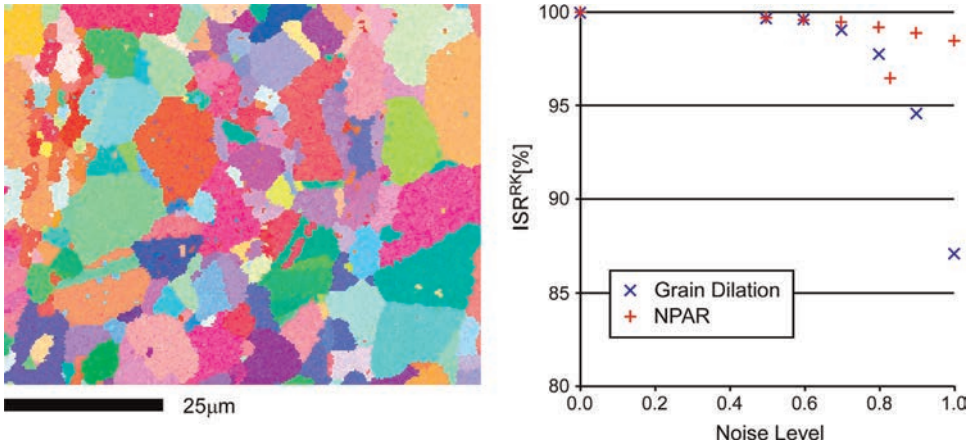

Fig. 7. Orientation map for the 1.0 noise level data after application of full grain dilation cleanup and a plot of ISR^{RK} vs noise level for NPAR and grain dilation cleanup.

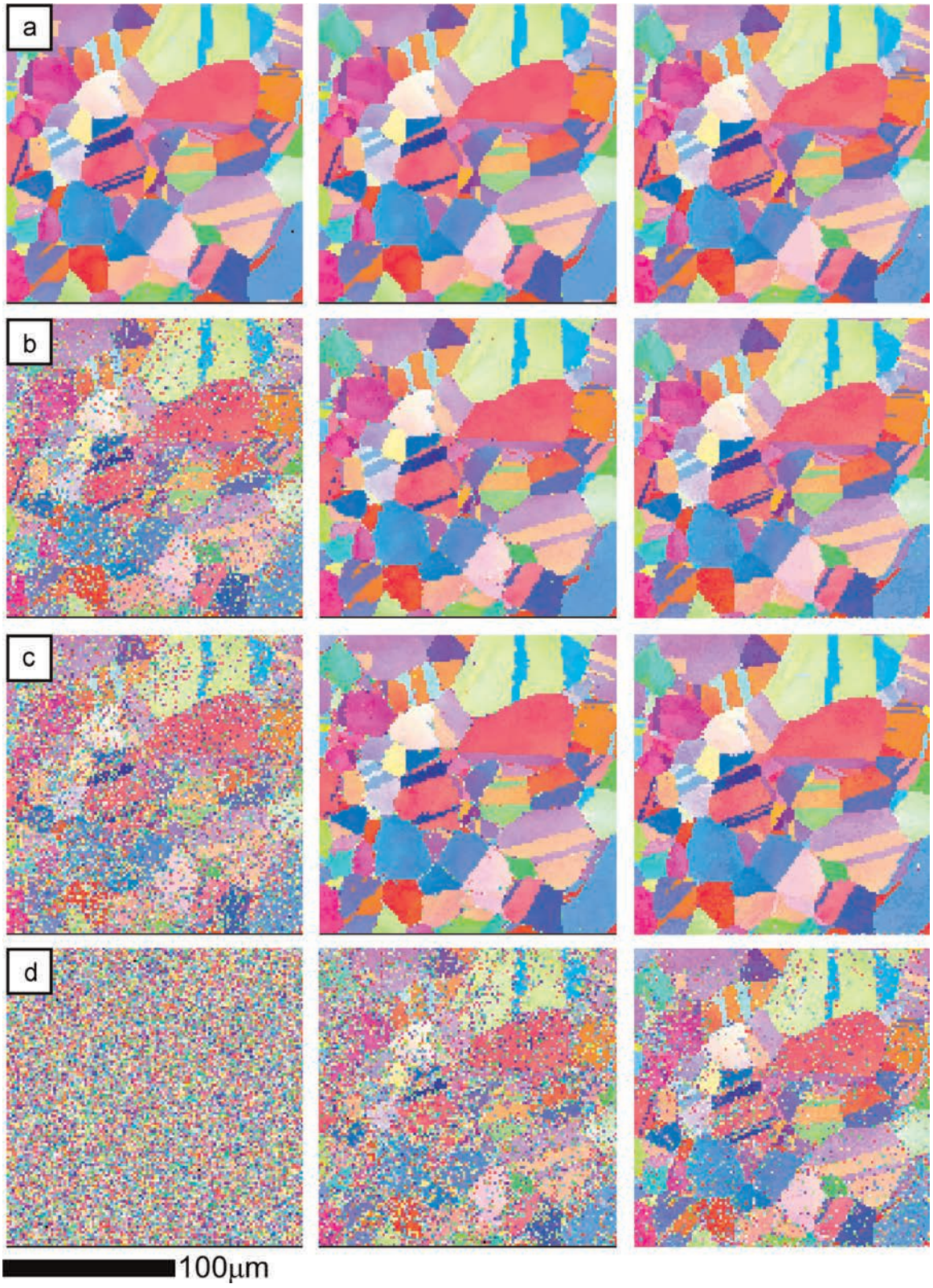

Fig. 8. Orientation maps for the nickel sample with increasingly noisy camera conditions for the gain at (a) 0, (b) 29.3, (c) 30.4 and (d) 36.0 dB. The orientation maps from left to right are for the as-scanned data, after NPAR and for the dictionary method.

whereas the re-assigned orientation is more likely to be included. Since the assigned orientation is a secondary solution it is expected to be less precise than the top solution thereby increasing the local KAM.

4.1.5. Comparison with grain dilation cleanup

Fig. 7 shows the orientation map after full grain dilation of the conventional rescan of the patterns with a 1.0 level of added noise. A comparison of this map with the NPAR map in Fig. 3d shows

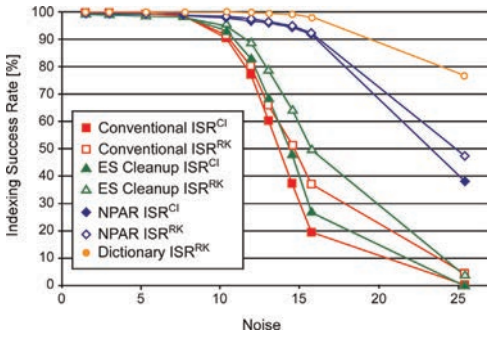

Fig. 9. Comparison of ISR metrics for the nickel sample for the conventionally re-scanned, ES Cleanup and NPAR, Dictionary data.

that, while the grain dilation does remarkably well given the scarcity of good data, the NPAR method produces a result more closely matching that obtained without any added noise which we assume is the most representative of the underlying microstructure. The grain shapes are more closely matched in the NPAR results than the grain dilation cleanup result. The grain dilation cleanup results also show a large number of extraneous island grains in the grain interiors. The improved fidelity of the map after NPAR relative to that obtained by the grain dilation cleanup is also evident in the plot of ISR^{RK} versus the noise level shown in Fig. 7.

4.2. NI with varied camera conditions

As described in Section 2.2, ten scans were collected under varying camera operating conditions. The noise associated with each camera condition was characterized by collecting a set of three background patterns at each camera condition while the beam is scanning. One pattern is subtracted from another and the standard deviation of the resulting intensity differences calculated. The calculation is restricted to the center portion of the pattern. For example, with a 60×60 pattern, a 30×30 mask is used. This was done to avoid edge effects and the area where there was no phosphor. This also concentrates the measurement on the area with the highest intensity; the noise is expected to increase radially away from this point. This calculation is repeated for each pair of patterns in the set of three and the average standard deviation ($\bar{\sigma}$) determined. This value is used to characterize the noise and ranged from 1.6 for the 0 gain data to 25.4 for the highest gain (36 db) data.

4.2.1. Mapping results

Fig. 8 shows a sampling of the sequence of ten scans. Orientation maps are shown in columns from left to right for the as-collected results, NPAR results and dictionary method results. The NPAR and dictionary methods clearly provide a large improvement in the high-gain data. The two methods produce comparable results except for the presence of more mis-indexed points at the grain boundaries in the NPAR data than in the dictionary data. At the noisiest condition, both the NPAR and dictionary methods start to show evidence for the presence of mis-indexed points at the grain boundaries and in the grain interiors.

4.2.2. ISR results

Fig. 9 shows a summary of the ISR results. The reference scan used was the as-scanned data at 0 dB. For the dictionary data the reference scan used was that dictionary result at zero gain. Because of a slight vertical drift over the entire sequence of scans it was necessary to increase the search kernel to second nearest neighbors for the dictionary ISR^{RK} values. This may lead to some inflation of the ISR^{RK} values but it is assumed the observed trends remain valid particular in the relative differences between the conventional, ES cleanup and NPAR results. It is clear that NPAR provides a dramatic improvement in the ISR values of the noisy patterns and that ES cleanup provides modest improvement. Once again, ISR^{CI} becomes more conservative with decreasing scan quality. This is because the CI standardization process only upgrades the CI values of those points which have neighbors of the same (or similar –within 5°) orientation. As the scan quality decreases, points which are correctly indexed are less likely to have neighbors with the same orientation and thus will not be upgraded during the CI standardization process. Zero solution type metrics are likely to over-estimate the ISR as the scan quality decreases because such metrics are based solely on points for which no orientation is obtained and do not account for mis-indexing which is likely to occur with more frequency as the general pattern quality diminishes.

4.2.3. Selective NPAR

A close inspection of the maps shown in Fig. 8 reveals one negative aspect of the NPAR results is that fine features such as very narrow twins are eliminated. This is due to an effective loss of spatial resolution in the averaging technique. One method to overcome this problem during the pattern averaging process is to only average the pattern of the current point with patterns from

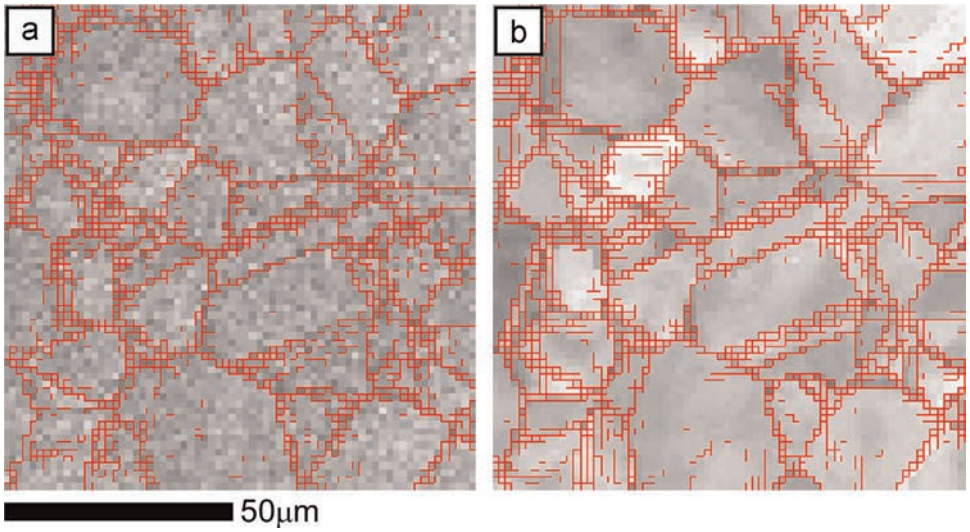

Fig. 10. Pattern difference boundaries greater than (a) 0.9 for the 29.3 dB gain level data and (b) 0.1 for the 0 dB gain scan overlaid on maps of pattern quality.

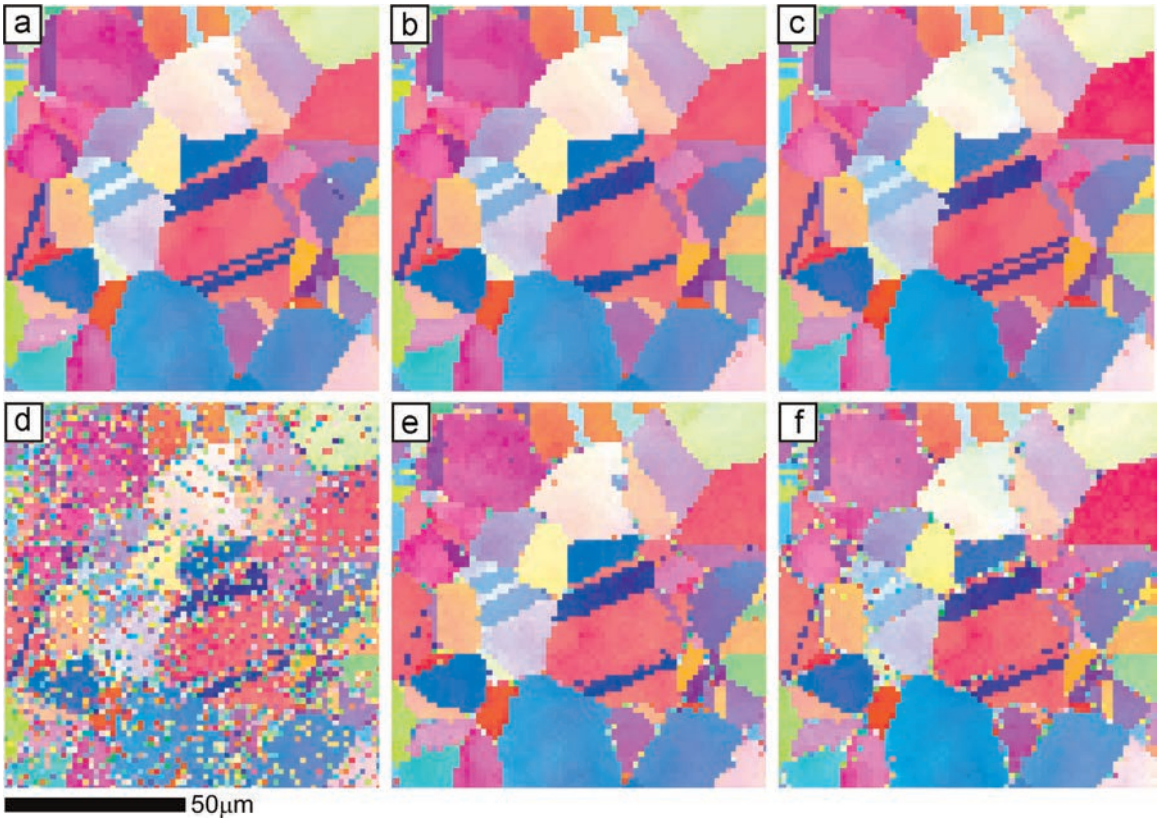

Fig. 11. Orientation maps for the (a) as-scanned, (b) NPAR rescan and (c) selective NPAR rescan for the 0 dB gain scan. Orientation maps for the (d) as-scanned, (b) NPAR rescan and (c) selective NPAR rescan for the 29.3 dB gain scan.

the neighboring points when the patterns are similar. This can be done using a pattern difference metric as outlined in [14]. The calculation is done by first normalizing the patterns by subtracting the overall average intensity of the pattern from each pixel in the pattern. The pattern intensities are then converted to a column vector and normalized. The pattern difference is then one minus the dot product of the two patterns. In order to find a good tolerance value we have used pattern quality maps overlaid with boundaries based on this pattern difference metric as shown in Fig. 10 for the top-left quarter of Fig. 8. Fig. 10a is for the scan at 29.3 dB and Fig. 10b is for the scan without any applied gain. A value of 0.9 was found to work well for the 29.3 dB scan and 0.1 for the 0 dB gain scan.

Fig. 11 shows orientation maps for the corresponding regions shown in Fig. 10 for a conventional, nearest neighbor averaged and selective nearest neighbor averaged re-scans for high and zero camera gains. The selective nearest neighbor averaging clearly reproduces the narrow twins again in the high-fidelity map and also somewhat in the noisier data. Unfortunately where NPAR is most effective (i.e. the high noise condition) selective NPAR provides only limited improvement in recovering the narrow twins but at the cost of less general noise reduction in the rescan. At this juncture, we have not identified a clear choice for the tolerance angle but have found a need to use the maps like those shown in Fig. 10 to optimize the tolerance scan for each new map. Not only is the value sensitive to the pattern noise as is evident in Fig. 10, but also to the pixel resolution.

Another approach would be to weight the averaging according the pattern difference measure – this would eliminate the need to preselect a tolerance value. This has been done by weighting the patterns by one minus the pattern difference metric during the averaging scheme. Unfortunately, the results from this weighting were not nearly as good as those obtained using the tolerance based method producing only a slight improvement over straight pattern averaging. This is most likely due to the lack of a strong correlation between the pattern difference metric and misorientation.

4.2.4. Expanded neighbor averaging

The effect of averaging over extended neighborhoods was also explored. Nearest neighbor averaging was carried out to the 5th nearest neighbor. Results are shown in Fig. 12 for three of the scans. In this figure the diagonal neighbors in each of the neighborhoods are included in the pattern averaging.

Fig. 13 shows the corresponding ISR results. In this case the horizontal axis is the number of points in the neighborhood averaging kernel. The most left-hand points in the plots is for the averaging without the diagonal neighbors, followed by including the diagonal neighbors for the 1st–5th nearest neighbors. It is clear that extending the number of neighbors included in the pattern averaging kernel helps but only out to the 2nd (or the 3rd for the noisiest data) nearest neighbors, after that it is a case of diminishing returns both in terms of the indexing success rate but also in terms of capturing higher-resolution features like twins. For example, in the results for the 3rd nearest neighbor kernels, the twins have completely disappeared due to averaging of the patterns from the twin with the patterns from the parent grain leading to the mixed patterns being dominated by the pattern from the parent. The appearance of zero solution data (colored black) with the larger kernel sizes suggests that over-averaging leads to patterns so smeared out that they are absent of diffraction bands detectable by the Hough transform. While the trend of an increase in ISR with additional neighbor followed by a decrease would be expected in all cases, the actual-turnover point in the curves is likely to be a function of the ratio between the step size and the average grain size. It should be noted that the data

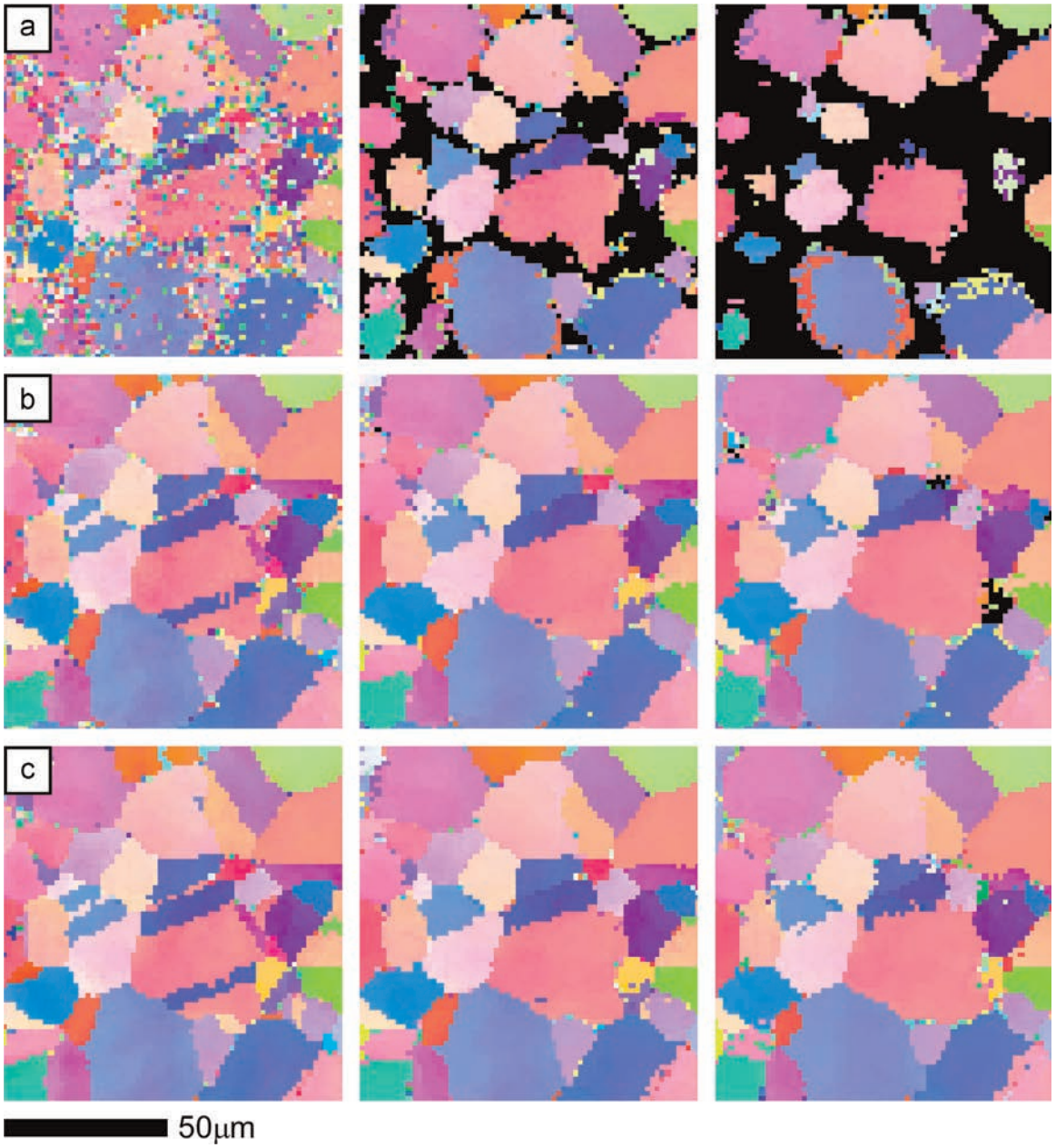

Fig. 12. Orientation maps of the (a) 36 dB, (b) 30.4 dB and (c) 27.0 dB gain scan for (from left-to right) 1st, 3rd and 5th nearest-neighbor NPAR results. Black points represent zero solution data points.

examined here was collected on a square grid. With a hexagonal grid, there are six equidistant nearest neighbors as opposed to four for the square grid leading to additional noise reduction in the averaging process for first nearest neighbor NPAR.

4.3. Deformed magnesium sample

4.3.1. Mapping results

The NPAR technique was applied to scan data obtained on a heavily deformed magnesium sample. The was from a twin roll cast AZ31 magnesium sheet that was hot rolled at 400 °C to 40% reduction. The sample was prepared first by mechanical polishing and then by grazing angle broad-beam ion etching. Fig. 14 shows the results for the as-scanned data and that re-scanned using NPAR. These maps show that NPAR does provide some improvement over the as-scanned data. However, the improvement is not nearly as dramatic as that obtained in the recrystallized nickel samples – a 10% improvement in the fraction of points indexed. Two areas were scanned. Area 1 was scanned with a camera gain of 0 and area 2 with a higher gain setting. The maps displayed in Fig. 14 are for area 2; only points with CI values greater than 0.1 after CI standardization are displayed in color those with CI less than 0.1 are shown in black. In this case the ISR^{CI} improves from 62.8% to 73.9% by performing the NPAR process. In area 1, the change in ISR^{CI} is more modest changing from 73.5% to only 76.2%. It should be noted that this sample exhibited some surface roughness introduced during broad-beam ion etching of the sample surface. While NPAR helps with the general quality of the patterns it is not expected to provide any substantial correction for surface topography effects on pattern quality and, in fact, will degrade the quality of a pattern for a point producing a good pattern by averaging it with poor or non-existent patterns from adjacent points. One approach to alleviating this problem would be to weight the patterns by the image quality in the averaging

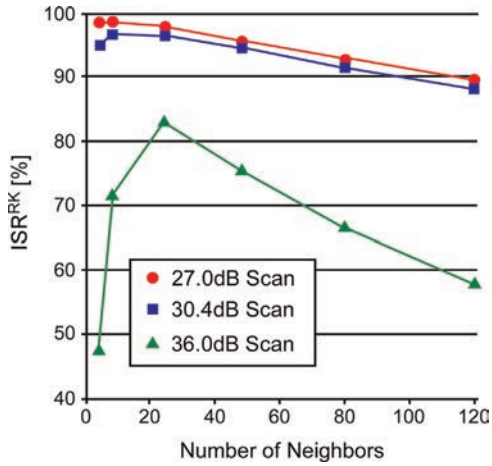

Fig. 13. ISR^{RK} results as a function of the number of points in the NPAR kernel.

procedure. It was found that this provided a 1% improvement in the ISR^{CI} over the standard non-weighted NPAR.

4.3.2. Merging results

Fig. 15 shows a higher magnification view of the region highlighted in the maps shown in Fig. 14. As expected, some detail is lost when NPAR is used due to the local pattern averaging in regions of fine structure. Local pattern averaging is in essence a virtual expansion of the interaction volume. The third map in the Fig. 15c is a merger of the conventional and NPAR scans where the point retained is that with the higher CI value. The merged data shows a higher fraction of indexed points but with the retained fine high resolution structure. Table 3 shows the ISR results for the data. Essentially the CI selective merger allows for a larger interaction volume to be used when it is advantageous and a smaller one when it is needed for a finer structure. For areas 1 and 2 the resulting ISR^{CI}s after the mergers were 82.7% and 77.6% respectively. It is interesting to note that in area 1 where the gain in indexing rate from NPAR was quite modest, the gain in the indexing rate from the CI merger process was greater than in area 2.

It should be noted that another approach could be pursued which would lead to a very similar result. That is, to only perform NPAR on points in the original scan with CI values less than a given tolerance value.

4.4. Fine-grained piano wire sample

4.4.1. Mapping results

Two scans were performed on a fine grained piano wire sample. The first scan was performed at a rate of 54 PPS and the second at 154 PPS. The second scan was scanned at a faster rate in an effort to reduce the amount of drift during the scanning process. The second scan was not over the same area but a nearby area in the sample. Two pairs of maps are displayed in Fig. 16 showing the as-scanned data at the two different scan rates. The first map in the pair shows all data points and the second shows only those data points with CI greater than 0.1 after CI standardization. Fig. 17 shows the NPAR results for the same pair of scans. Points colored black in the (a) and (c) portions of these figures are points for which no indexing solution was found. In (b) and (d) the points colored black are those with CI values less than 0.1. The maps show a modest improvement using NPAR over the conventional scanning approach.

The indexing results for these two scans are summarized in Table 4. The ISRs shows that there is potentially more improvement in the scan data than can be recognized by simply comparing the maps – nearly 20% in the 54 PPS case and over 15% in the 154 PPS case. Once again, the CI merger process enables a further step in improving the overall scan fidelity.

4.4.2. Comparison with grain dilation cleanup

Fig. 18 shows the result after applying a single iteration of the grain dilation cleanup process to the conventional scan data. A comparison of this map to Fig. 17d clearly shows that the NPAR results are substantially better than can be obtained using grain dilation cleanup. It should be noted that the cleanup routine modified the orientations of 22.3% of the points in the scan; whereas, NPAR increased the number of validly indexed points by 26.3%, i.e. the ISR^{CI} increased by 26.3%

4.4.3. Drift

The 54 PPS scan underwent a substantial amount of drift during the duration of the scan. If linear drift is assumed, which is generally a big assumption when the drift is due to charging on the sample surface, then we see a drift of about 270 nm in the horizontal direction and 1620 nm in the vertical direction. In the 154 PPS scan we see a drift of only 62 nm in the horizontal and 645 nm in the vertical. In a fine-grained sample such as this, where the resolution limits of the technique are being pushed, the NPAR technique provides an opportunity to operate the camera in a faster condition mitigating drift effects while still allowing good

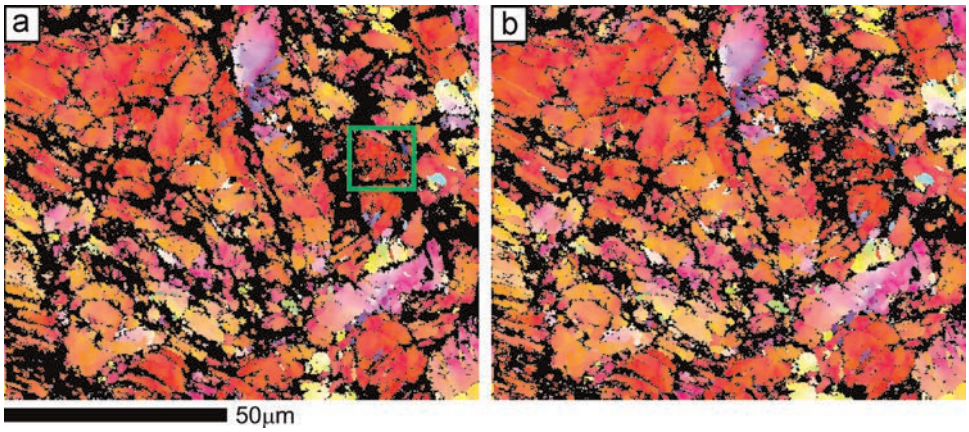

Fig. 14. Orientation maps of the (a) as-scanned and (b) NPAR data from the deformed Mg sample.

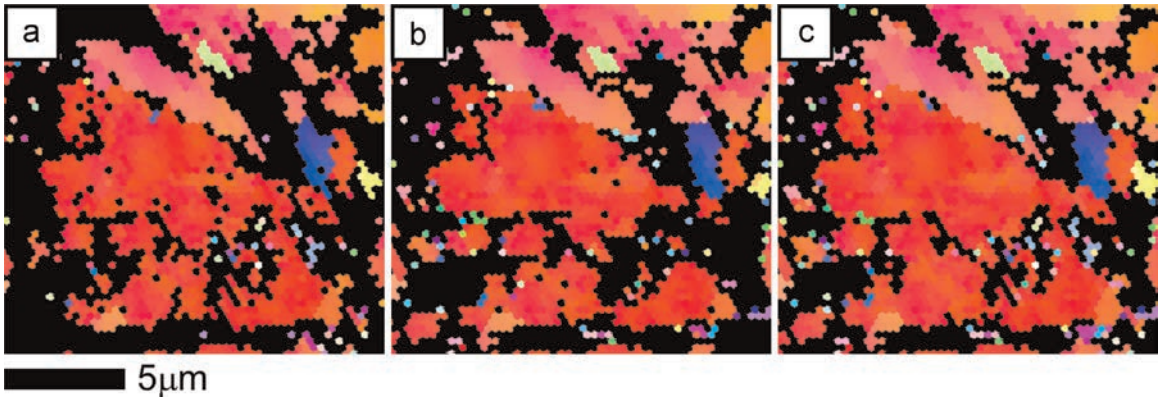

Fig. 15. Orientation maps of the (a) as-scanned, (b) NPAR and (c) CI merged data on the deformed Mg sample.

Table 3
Average KAM values for the different post-processing methodologies and noise levels.

Area	Conventional ISR^{CI} (%)	NPAR ISR^{CI} (%)	Merged ISR^{CI} (%)
1	73.5	76.2	82.7
2	62.8	73.9	77.6

data to be collected on a fine scan grid. In theory, going faster means shorter dwell times and less contamination and charging. In fact, in this case the drift rate in the vertical direction was actually slightly less (12%) for the slower scan but significantly more for the horizontal direction (52%). The second scan area was only shifted a few microns away from the first scan area. It is conceivable that the charging effects remaining in the first area influenced the drift rate in the second leading to the observed increase in drift rate in the second scan.

5. Conclusions

The NPAR technique can produce dramatic improvements on the indexing success rate and spatial fidelity of the resultant maps over conventional methods. It also provides improved orientation precision as evidence by smaller KAM values (in the recrystallized nickel samples). However, these improvements are best realized

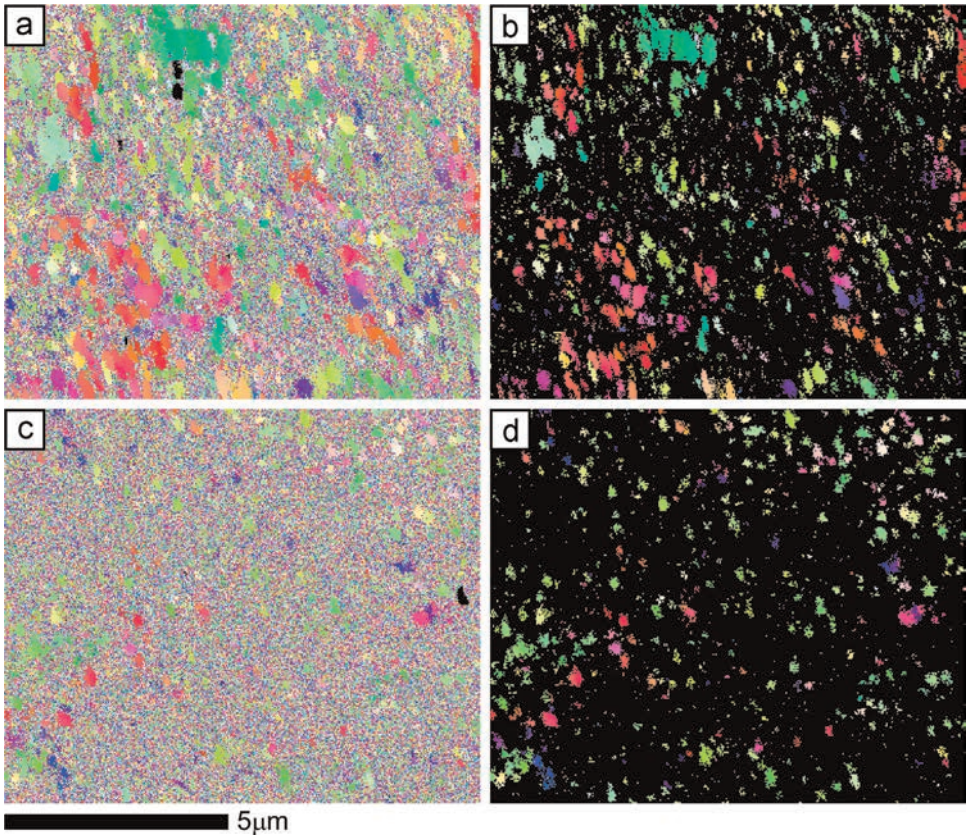

Fig. 16. Orientation maps for (a and b) 54 PPS scan and (c and d) 154 PPS scan on the fine-grained sample. In (b) and (d) the points in black have CIs less than 0.1 after CI standardization.

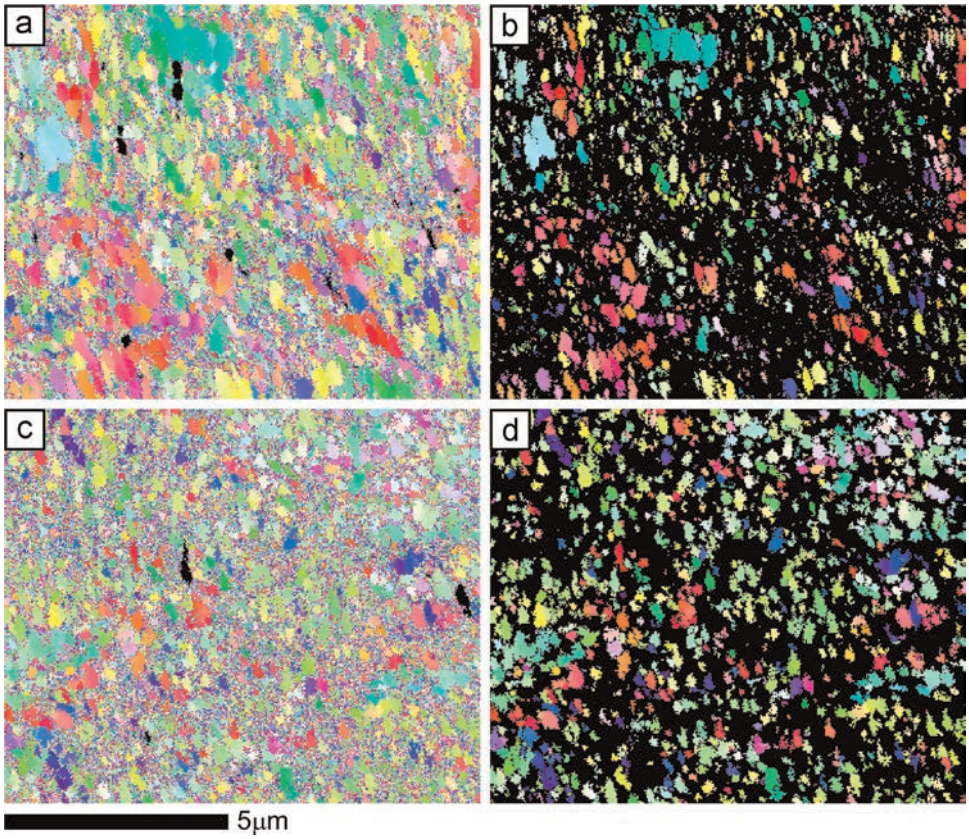

Fig. 17. Orientation maps for (a and b) 54 PPS scan and (c and d) 154 PPS scan on the fine-grained sample after NPAR. In (b) and (d) the points in black have CIs less than 0.1 after CI standardization.

Table 4
ISR^{CI} results for the piano wire sample.

Scan speed	Conventional rescan (%)	ES cleanup (%)	NPAR (%)	CI merger (%)
54 PPS	34.9	41.3	54.1	59.7
154 PPS	9.3	12.5	35.6	37.6

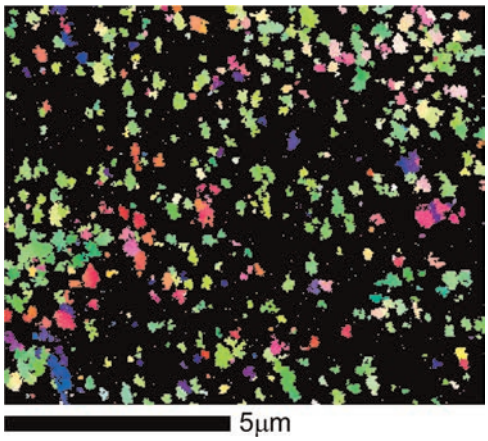

Fig. 18. Orientation map after a single iteration of grain dilation cleanup on the as-scanned data.

on relatively straightforward materials (from an EBSD perspective) where noisy patterns are a result of high gain camera conditions such as are used in low beam current situations or when optimizing for speed such as is often done in in-situ work or collecting serial section data for three-dimensional characterization as opposed to noisy patterns due to inherent challenges in the sample itself such as limitations due to high-resolution microstructural features such as fine twins or small islands composed of second phase precipitates.

It was found in the deformed sample that selective merging of the results from conventional scanning with the NPAR results allows for improved indexing rates while retaining good characterization of the fine structure inherent to deformed materials. Other weighting schemes were also observed to be beneficial in improving indexing rates and retaining areas with fine structure but with only modest gains compared to selective merging.

NPAR generally improves pattern quality and can be thought of in two ways: first, as virtual frame averaging but without the associated time penalty; and second, as a virtual increase in the interaction volume with an inherent loss in spatial resolution. With coarser scan resolutions relative to the underlying grain structure, the spatial resolution penalty becomes more pronounced.

ES cleanup provides a moderate boost to the indexing rate but can be used when EBSD patterns are not stored during the scanning process, but does require that the extra solutions be recorded during the original scan.

A tangential benefit of this study was the confirmation of using the fraction of points with CI values greater than some tolerance value (0.1 in this case) as a good means of assessing the indexing success rate. By comparing the CI fraction approach to a reference scan comparison approach it was found that the CI fraction based metric tends towards being slightly conservative with decreasing scan quality. While it would be better if the metric were consistent with indexing quality, confirming that the error tends towards the conservative fortunately validates its longstanding use in the EBSD community.

While not a focus of this work, it should be noted that the dictionary method provides excellent results even in very noisy conditions.

Acknowledgments

We acknowledge our former colleague at EDAX, Reinhard Buchold, for devising the pattern noise metric used in Section 4.2. MDG would like to acknowledge the Air Force Office of Scientific Research, MURI contract #FA9550-12-1-0458, for financial support.

References

[1] A.J. Schwartz, M. Kumar, B.L. Adams, D.P. Field, Electron Backscatter Diffraction in Materials Science, second ed., Springer, New York, 2009.
[2] B.L. Adams, S.I. Wright, K. Kunze, Orientation imaging: the emergence of a new microscopy, Metall. Trans. A 24 (1993) 819–831.
[3] S.I. Wright, B.L. Adams, Automatic-analysis of electron backscatter diffraction patterns, Metall. Trans. A 23 (1992) 759–767.
[4] K. Kunze, S.I. Wright, B.L. Adams, D.J. Dingley, Advances in automatic EBSP single orientation measurements, Texture Microstruct. 20 (1993) 41–54.
[5] F.J. Humphreys, Review-grain and subgrain characterization by electron backscatter diffraction, J. Mater. Sci. 36 (2001) 3833–3854.
[6] S.I. Wright, Random thoughts on non-random misorientation distributions, Mater. Sci. Technol. 22 (2006) 1287–1296.
[7] Y.H. Chen, S.U. Park, D. Wei, G. Newstadt, M.A. Jackson, J.P. Simmons, Marc De Graef, A.O. Hero, A dictionary approach to Electron Backscatter Diffraction Indexing, iMicrosc. Microanal 21 (2015) 739–752.
[8] S.I. Wright, EDAX blog, November 2014. ⟨http://edaxblog.com/2014/11/18/tuning-the-microstructure⟩.
[9] D.P. Field, Recent advances in the application of orientation imaging, Ultramicroscopy 67 (1997) 1–9.
[10] M.M. Nowell, S.I. Wright, Orientation effects on indexing of electron backscatter diffraction patterns, Ultramicroscopy 103 (2005) 41–58.
[11] S.I. Wright, M.M. Nowell, R. de Kloe, L. Chan, Orientation precision of electron backscatter diffraction measurements near grain boundaries, Microsc. Microanal. 20 (2014) 852–863.
[12] E.M. Lehockey, Y.P. Lin, O.E. Lepik, Mapping residual plastic strain in materials using electron backscatter diffraction, in: A.J. Schwartz, M. Kumar, B.L. Adams (Eds.), Kluwer Academic/Plenum Publishers, New York, 2000, pp. 247–264.
[13] S.I. Wright, M.M. Nowell, D.P. Field, A review of strain analysis using electron backscatter diffraction, Microsc. Microanal. 17 (2011) 316–329.
[14] S.I. Wright, I. Stuart, M.M. Nowell, R. de Kloe, P. Camus, T. Rampton, Electron imaging with an EBSD detector, Ultramicroscopy 148 (2015) 132–145.